ACS OMEGA

http://pubs.acs.org/journal/acsodf

Article

Surface Functionalization of Graphene Oxide with Hyperbranched Polyamide-Amine and Microcrystalline Cellulose for Efficient Adsorption of Heavy Metal Ions

Zhihang Liu, Qian Wang, Xiujie Huang,* and Xueren Qian

Cite This: *ACS Omega* 2022, 7, 10944−10954

Read Online

ACCESS | Metrics & More | Article Recommendations

ABSTRACT: Graphene oxide (GO)-based adsorbents have received attention in the removal of heavy metal ions in wastewater due to its large specific surface area and oxygen-containing functional groups, which can enhance the interaction between GO and heavy metal ions. Many researchers are seeking economical and effective strategies to further improve the adsorption capacity of GO. In this study, hyperbranched polymers and cellulose were used to surface functionalize GO for the efficient adsorption of heavy metal ions. First, hyperbranched polyamide-amine (HPAMAM) functionalized GO was fabricated by the formation of an amide bond between the carboxyl group of GO and the amino group of HPAMAM, increasing the active groups on the GO surface and enhancing the affinity with heavy metal ions. Then, dialdehyde cellulose (DAC) obtained through the oxidation of microcrystalline cellulose was grafted onto GO/HPAMAM by forming a Schiff-based structure between the amino group of HPAMAM and aldehyde group of DAC. Interestingly, DAC formed micro/nano bumps on GO, which was beneficial to increase the hydroxyl number and contact area with heavy metal ions. The Fourier-transform infrared spectroscopy (FT-IR), X-ray diffraction (XRD), X-ray photoelectron spectroscopy (XPS), thermogravimetric analysis (TGA), and scanning electron microscopy (SEM) results confirmed the successful synthesis of GO/HPAMAM/DAC. The obtained GO/HPAMAM/DAC adsorbent exhibited strong adsorption capacity and good cycle stability for heavy metal ions. The maximum adsorption capacities of Pb(II), Cd(II), and Cu(II) were 680.3, 418.4, and 280.1 mg/g at 298 K, which were better than those of most adsorbents reported. A pseudo-second-order kinetic model could well-describe the Pb(II), Cd(II), and Cu(II) adsorption onto GO/HPAMAM/DAC, and the equilibrium data fitted well with the Langmuir isotherm model. The adsorption of Pb(II), Cd(II), and Cu(II) was mainly attributed to the chelation or complexation of nitrogen- and oxygen-containing groups on the GO/HAPAMAM/DAC adsorbent. This study may provide a novel strategy for improving the adsorption performance of GO with hyperbranched polymers and cellulose.

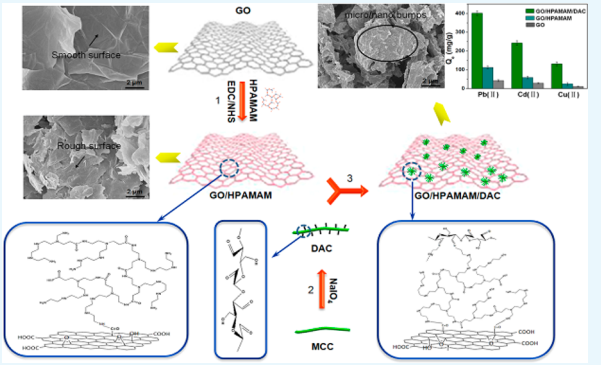

INTRODUCTION

With the global industrial development, heavy metal ions are used in many fields, such as light industry, batteries, and electroplating. Industrial wastewater contains many heavy metal ions.[1] Considering its high toxicity, low degradation, and easy bioaccumulation of heavy metal ions,[2] it is important to remove heavy metal ions from wastewater to avoid threats to the ecosystem and human health. Presently, membrane separation, chemical precipitation, photocatalysis, reverse osmosis, adsorption and other technologies have been used to remove heavy metal ions from wastewater.[3,4] Among them, adsorption has the advantages of high efficiency, convenience, and easy industrial amplification and is widely used in wastewater treatment.[5,6] Recently, carbon-, polymer-, and biomass-based adsorbents have been designed to achieve low-cost and efficient heavy metal-ion adsorption.[7] Among them, graphene with one carbon atom thick has received increasing attention as an adsorbent.

Graphene has unique electrochemical properties, excellent mechanical and thermal properties, and a large specific surface area.[8] The oxidized graphene contains oxygenous groups, such as hydroxyl and carboxyl groups, which increases the hydrophilicity and the interaction with heavy metal ions.[9] Therefore, graphene oxide (GO) is considered to be a promising adsorbent for the adsorption of heavy metal ions. The adsorption performance of the GO-based adsorbent

Received: November 23, 2021
Accepted: March 11, 2022
Published: March 23, 2022

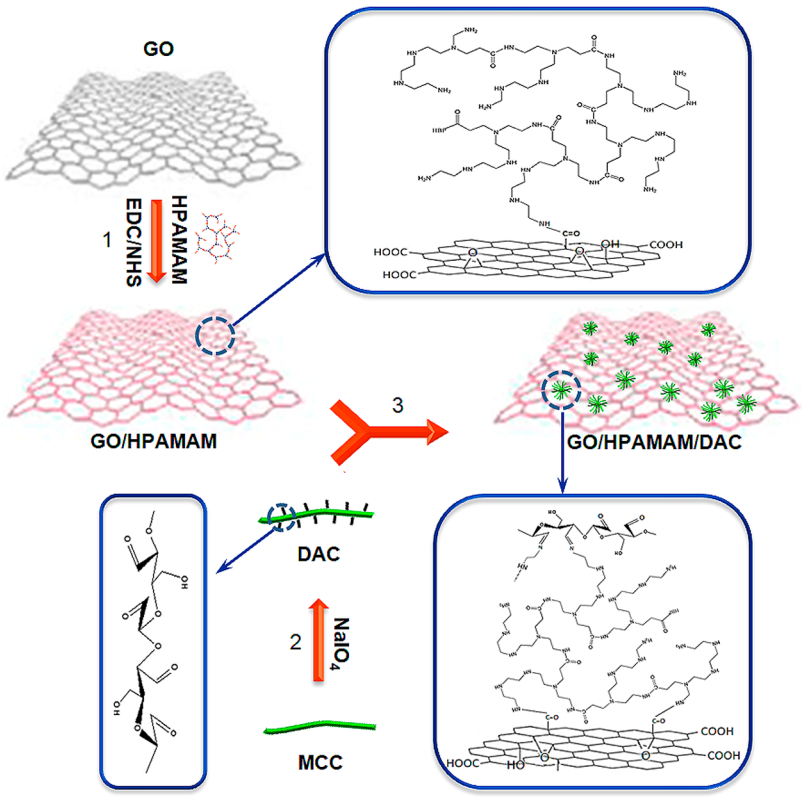

Figure 1. Schematic of the synthesis of the GO/HPAMAM/DAC adsorbent.

depends on the contact area, hydrophobic effects, energy surface sites, affinity with pollutants, and adsorption environment (such as pH and temperature).[10−12] Researchers are committed to modifying GO for more efficient adsorbents. The design of advanced GO-based adsorption materials should follow two principles: (1) introduce more active groups on the GO surface to enhance its affinity with heavy metal ions and (2) increase the contact area of GO with pollutants for an efficient adsorption process.

Hyperbranched polymers have abundant terminal active groups and many internal cavities formed by branched molecular structures.[13] Hyperbranched polyamide-amine (HPAMAM) presents a spherical branched molecular structure with developed nanocavities and many terminal amino groups.[14] Adsorbents with nitrogen-chelating ligands, such as amino groups, are more efficient in adsorbing heavy metal ions.[15−17] Yu et al.[18] grafted hyperbranched polyamide onto a cellulose surface for enhancing its adsorption performance. Xue et al.[19] prepared a cellulose-based adsorbent by cross-linking microcrystalline cellulose with amino-terminated hyperbranched polymers. In this study, HPAMAM was grafted onto GO by forming an amide bond between the amino group of HPAMAM and the carboxyl group of GO. The introduction of a large number of active groups onto GO by grafting HPAMAM is beneficial to enhance the affinity with heavy metal ions. In order to further enhance the adsorption performance of GO, a strategy is needed to increase the contact area of GO with pollutants for an efficient adsorption process.

Due to its biocompatibility, degradability, low cost, and being rich in hydroxyl groups, cellulose is considered as an ideal adsorption material for heavy metal ions. Zhao et al.[20] prepared a cellulose hydrogel by cross-linking acrylamide and acrylic acid for heavy metal ions adsorption. Qiao et al.[21] synthesized a porous cellulose sphere by a preliminary chemical cross-linking strategy for heavy metal ions adsorption. Cellulose can also combine with GO dispersed in an aqueous medium through hydrogen bonding.[22] The grafting of cellulose on GO increases the hydroxyl number and contact area with pollutants, which creates favorable conditions for effective adsorption. On the contrary, the introduction of cellulose can reduce the cost of GO-based adsorbents. Zhang et al.[23] reported a porous GO/carboxymethyl cellulose adsorbent prepared using a unidirectional freeze-drying method, which was efficient in the adsorption of Ni^{2+}. Zaman et al.[24] combined microcrystalline cellulose (MCC) obtained from waste jute with GO through a modified Hummers' method to construct GO/MCC nanocomposite adsorbent. Therefore, hyperbranched polymers and cellulose are expected to improve the adsorption performance of GO by surface grafting.

In this study, HPAMAM and MCC were used to surface functionalize GO for the efficient adsorption of heavy metal ions. HPAMAM was grafted onto GO via an amide bond, and dialdehyde cellulose (DAC) obtained by the oxidation of MCC was grafted on HPAMAM by forming a Schiff-based structure. Thus, HPAMAM and DAC were expected to increase the active groups and specific surface area of GO for an efficient adsorption process. The synthesized GO/HPAMAM/DAC was used as an adsorbent for the adsorption of heavy metal ions in water. Pb(II), Cd(II), and Cu(II) were selected as model pollutants to determine the adsorption efficiency of adsorbents. The adsorption kinetics, adsorption type, adsorption isotherm, adsorption capacity, adsorption cycle, and adsorption mechanism were ascertained.

https://doi.org/10.1021/acsomega.1c06647
ACS Omega 2022, 7, 10944−10954

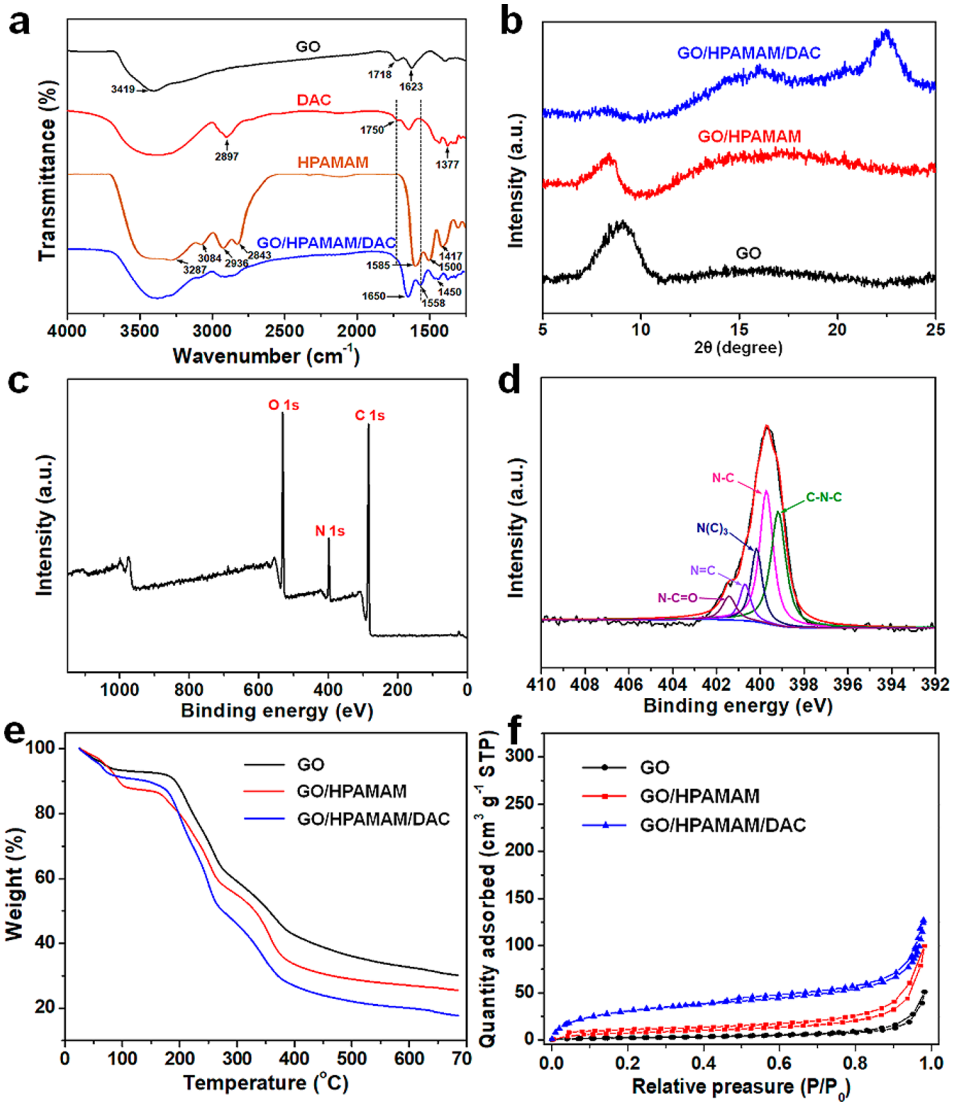

Figure 2. (a) FT-IR spectra of GO, DAC, HPAMAM, and GO/HPAMAM/DAC. (b) XRD patterns of GO, GO/HPAMAM, and GO/HPAMAM/DAC. (c) Full X-ray photoelectron spectroscopy (XPS) spectrum of GO/HPAMAM/DAC, and high-resolution XPS spectrum of (d) N 1s. (e) Thermogravimetric analysis (TGA) profiles of GO, GO/HPAMAM, and GO/HPAMAM/DAC. (f) N_2 adsorption−desorption isotherm of GO, GO/HPAMAM, and GO/HPAMAM/DAC.

RESULTS AND DISCUSSION

Proposed Process Concept of GO Surface Functionalization with HPAMAM and MCC. In order to further improve the adsorption capacity of GO, this study proposes to introduce HPAMAM and MCC on the surface of GO to increase the contact area and affinity between the adsorbent and pollutants. The HPAMAM and MCC functionalized GO adsorbent was prepared through the synthesis process shown in Figure 1. It involves the following steps: (1) HPAMAM was grafted onto GO by forming an amide bond in the presence of a catalyst (EDC/NHS) to increase the number of active groups. (2) MCC was oxidized to DAC using $NaIO_4$ for introducing aldehyde groups on the cellulose molecular chain, which would create conditions for the grafting of DAC on GO/HPAMAM. (3) The DAC was grafted onto GO/HPAMAM by forming a Schiff-based structure between the amino group of HPAMAM and the aldehyde group of the DAC to construct micro/nano bumps on the surface of GO.

Characterization of GO/HPAMAM/DAC Adsorbent. First, Fourier-transform infrared spectroscopy (FT-IR) spectra were carried out to confirm the covalent grafting of HPAMAM and DAC on GO. Figure 2a shows the FT-IR spectra of GO, DAC, HPAMAM, and GO/HPAMAM/DAC. For GO, the stretching vibration peaks of C═C, C═O, and —OH appeared at 1623, 1718, and 3419 cm^{-1}, respectively.[25] For HPAMAM, the bending vibration peak of —CH_2— appeared at 1417 cm^{-1}.[17] The —NH— flexural vibration peak and —C═O tensile vibration peak of the amide bond appeared at 1500 and 1585 cm^{-1}, respectively. The symmetric and asymmetric tensile vibration peaks of —CH_2— appeared at 2843 and 2936 cm^{-1}. The tensile vibration peak of —NH_2 appeared at 3084 cm^{-1}. The broad peak at 3287 cm^{-1} was attributed to the superposition of the —NH— stretching vibration peak of the amide bond and the —NH_2 stretching vibration peak. For DAC, the C═O stretching vibration peak of the aldehyde group appeared at 1750 cm^{-1},[26] confirming the introduction of the aldehyde group on the cellulose molecular chain after oxidation. In contrast, some new peaks appeared in

https://doi.org/10.1021/acsomega.1c06647
ACS Omega 2022, 7, 10944−10954

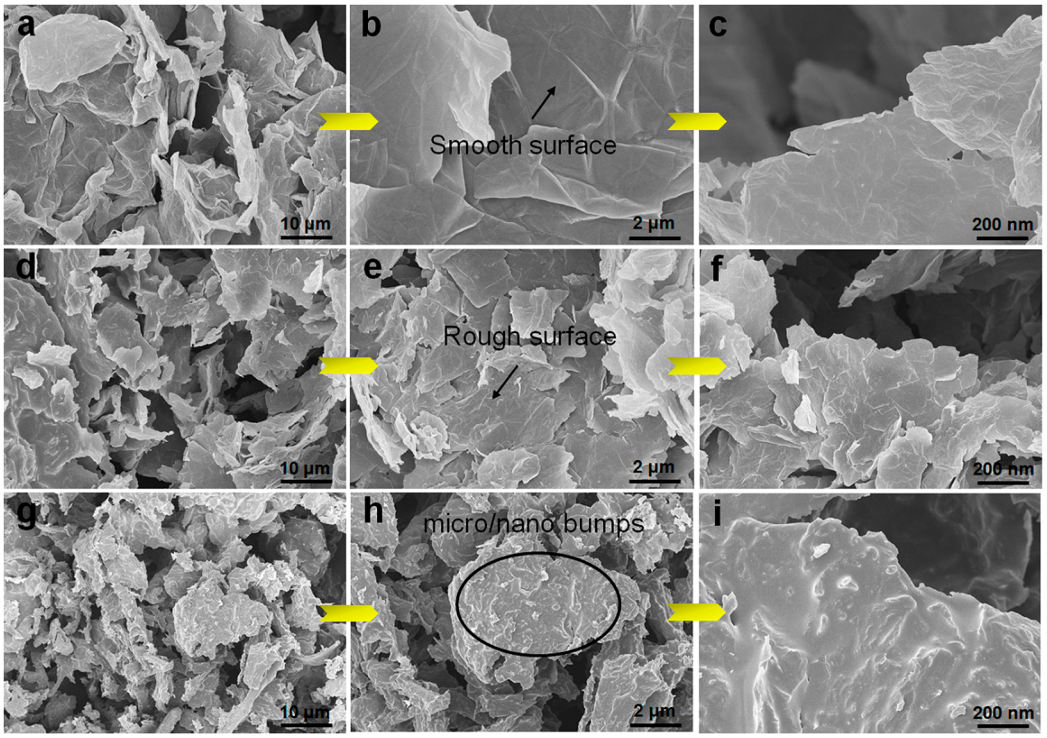

Figure 3. Scanning electron microscopy (SEM) images of (a–c) GO, (d–f) GO/HPAMAM, and (g–i) GO/HPAMAM/DAC.

GO/HPAMAM/DAC. The peaks at 1450, 1650, and 3380 cm^{-1} correspond to the vibrations of —CH_2—, —CONH—, and —NH—, respectively,[27] confirming the graft of HPAMAM on GO through an amide bond. On the contrary, the C═N vibration peak appeared at 1558 cm^{-1} and the C═O stretching vibration peak of the aldehyde group at 1750 cm^{-1} disappeared, which indicated the formation of a Schiff-based structure between the amino group of HPAMAM and the aldehyde group of DAC. Thus, DAC was covalently grafted onto the surface of GO with the help of HPAMAM.

Then, X-ray diffraction (XRD) spectra were performed to study the crystallographic structure of GO-based adsorbent after grafting HPAMAM and DAC. The XRD spectra of GO, GO/HPAMAM, and GO/HPAMAM/DAC are shown in Figure 2b. An intense peak at $2\theta = 9.08°$ for GO was caused by the interlayer spacing of GO sheets.[28] After grafting HPAMAM, the characteristic diffraction peak of GO was reduced, which may be due to the shielding of GO by HPAMAM. In addition, the characteristic diffraction peak of GO was further reduced after grafting DAC, and the characteristic diffraction peak corresponding to the typical crystalline structure of cellulose I appeared at about $2\theta = 23°$. The decrease in the crystallinity of GO may be due to the grafting of microcrystalline cellulose (about 90 μm of crystallite size), which resulted in the nonuniform content of GO.[29]

Subsequently, the surface chemical structure of GO/HPAMAM/DAC adsorbent was analyzed by X-ray photoelectron spectroscopy (XPS) spectra. As shown in Figure 2c, a distinct characteristic peak corresponding to N 1s appears at about 400 eV, which implies the grafting of HPAMAM in the adsorbent. This sharp peak indicates the relatively high nitrogen content in GO/HPAMAM/DAC. The high-resolution spectrum of N 1s is shown in Figure 2d. The characteristic peaks corresponding to C—N—C, C—N, $N(C)_3$, C═N, and N—C═O appeared at 399.2, 399.8, 400.1, 400.8, and 401.4 eV, respectively.[30] The appearance of N—C═O and C═N proved the grafting of HPAMAM and DAC on GO, which was consistent with the results of FT-IR spectra. The primary, secondary, and tertiary amines presented in GO/HPAMAM/DAC could promote the adsorption of heavy metal ions.

Next, the thermal stability and volatile portion of GO, GO/HPAMAM, and GO/HPAMAM/DAC were determined by thermogravimetric analysis (TGA) with a temperature range of 25–700 °C (as shown in Figure 2e). The weight loss between 100 and 130 °C was mainly due to the evaporation of adsorbed water. For GO, the weight loss between 200 and 250 °C was mainly due to the removal of oxygen-containing groups (such as carboxyl, carbonyl, and epoxy).[31] For GO/HPAMAM, there was a higher weight loss compared with GO. This was mainly attributed to the decomposition of the molecular chain of HPAMAM between 180 and 410 °C. After grafting DAC onto GO/HPAMAM, the weight loss was further increased, which was due to the cleavage of glycosidic bonds and other bonds (such as C—O, C—C) of cellulose at 240–400 °C.[32]

In order to determine the improvement effect of DAC grafting on the specific surface area of GO, N_2 adsorption isotherms of GO, GO/HPAMAM, and GO/HPAMAM/DAC were carried out (as shown in Figure 2f). GO, GO/HPAMAM, and GO/HPAMAM/DAC all had a H_3 hysteresis loop. This is characteristic of lamellar aggregates with irregularly shaped and sized slit shape pores. The specific surface areas of GO, GO/HPAMAM, and GO/HPAMAM/DAC were 87.5, 96.7, and 138.9 m^2/g, respectively. Obviously, GO presented a larger specific surface area after grafting HPAMAM and DAC. This once again proved that HPAMAM and DAC were successfully grafted on the surface of GO, and the grafted HPAMAM and DAC could change the surface structure of GO. The increased specific surface area was beneficial to increase the contact area

https://doi.org/10.1021/acsomega.1c06647
ACS Omega 2022, 7, 10944–10954

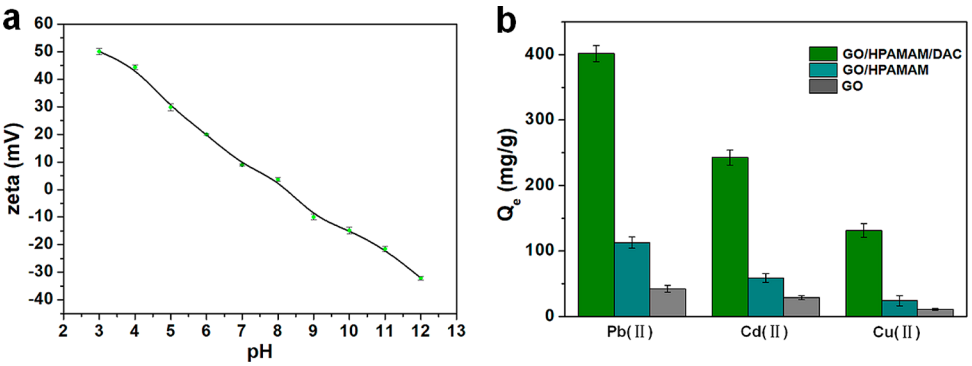

Figure 4. (a) ζ potentials of GO/HPAMAM/DAC adsorbent at various pH values (3.0−12.0). (b) Adsorption capacities of Pb(II), Cd(II), and Cu(II) on GO, GO/HPAMAM, and GO/HPAMAM/DAC (T = 298 K, t = 24 h, m = 10 mg, V = 100 mL, C_0^{metal} = 100 mg/L).

between the adsorbent and heavy metal ions for an efficient adsorption.

Finally, micrographs were taken to observe the morphological changes on the GO surface after grafting HPAMAM and DAC. The scanning electron microscopy (SEM) images of GO, GO/HPAMAM, and GO/HPAMAM/DAC are shown in Figure 3. The GO (Figure 3a−c) displayed a smooth sheet-layer structure with a certain degree of stacking. After HPAMAM was grafted (Figure 3d−f), GO showed a rough surface. This may be due to the branched molecular structure and the nanocavities of HPAMAM. The abundant active groups in HPAMAM could improve the affinity between adsorbents and heavy metal ions. In addition, the stacking degree of GO was reduced. After the grafting of DAC onto GO/HPAMAM (Figure 3g−i), the surface of GO became rougher and micro/nano bumps appeared. Hao et al.[33] prepared a GO-based adsorbent by mixing GO and cellulose in ionic liquid. The GO/cellulose composite exhibited a smooth phase. In this study, micro/nano bumps formed on GO after covalent grafting of cellulose on GO with the help of HPAMAM, which was beneficial to increase the contact area with pollutants for an efficient adsorption process.

Adsorption Performance of GO/HPAMAM/DAC Adsorbent. As shown in Figure 4a, the surface charge of GO/HPAMAM/DAC adsorbent in the pH range of 3.0−12.0 was analyzed. It was easy to find that the ζ potential of the adsorbent decreased with the increase of pH. When the pH was 8.24, the ζ potential was zero. Therefore, the isoelectric point (pH_{ip}) of GO/HPAMAM/DAC adsorbent was 8.24. The surface charge of GO/HPAMAM/DAC adsorbent was positive at pH < 8.24 because the primary and secondary amines in HPAMAM interacted with H^+ to form cationic groups.[26]

Figure 4b shows the adsorption capacity of the adsorbents for Pb(II), Cd(II), and Cu(II). The unmodified GO had the worst adsorption capacity (42.4, 28.7, and 10.8 mg/g for Pb(II), Cd(II), and Cu(II), respectively). After grafting HPAMAM, the adsorption capacity of GO/HPAMAM was improved (112.8, 58.9, and 24.3 mg/g for Pb(II), Cd(II), and Cu(II), respectively). This was mainly due to the introduction of more nitrogen- and oxygen-containing groups on GO, which enhanced the affinity between the adsorbent and heavy metal ions. After grafting DAC, the adsorption capacity of GO/HPAMAM/DAC showed more improvement (401.5, 242.8, and 131.4 mg/g for Pb(II), Cd(II), and Cu(II), respectively). The grafting of cellulose on GO increased the hydroxyl number and contact area with pollutants for an efficient adsorption process.

The pH has a great influence on the adsorption of heavy metal ions onto the adsorbent. On the one hand, pH will affect the charge loading on the solid/liquid interface, thereby affecting the adsorption process of heavy metal ions in the aqueous solution. On the other hand, pH affects the competitive adsorption between hydrogen ions and heavy metal ions. Figure 5 shows the effect of pH on the adsorption

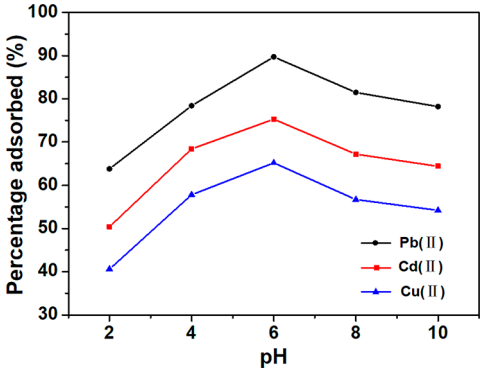

Figure 5. Effect of pH on the adsorption of Pb(II), Cd(II), and Cu(II) onto GO/HPAMAM/DAC (T = 298 K, t = 60 min, m = 300 mg, V = 50 mL, C_0^{metal} = 100 mg/L).

of Pb(II), Cd(II), and Cu(II) onto GO/HPAMAM/DAC. When the pH was 6.0, the best adsorption rates of Pb(II), Cd(II), and Cu(II) were 89.7%, 75.3%, and 65.2%, respectively. When the pH was lower than 6.0, a higher concentration of H_3O^+ ions would compete with heavy metal ions to occupy adsorption sites, resulting in the decrease of adsorption capacity. With the increase of pH, the protonation of the amino groups weakened, enhancing its coordination and chelating ability for heavy metal ions. But, when the pH was higher than 6.0, metal ions might precipitate, resulting in a poor adsorption effect. Figure 6 shows the effect of GO/HPAMAM/DAC dosage on the adsorption of Pb(II), Cd(II), and Cu(II). On the whole, the adsorption rate of heavy metal ions showed an increasing trend with the increase of adsorbent dosage. When the dosage of adsorbent was less than 100 mg, the curve showed a sharp rise. When the dosage of the adsorbent was higher than 100 mg, the curve showed a gentle rise. Parts a−c of Figure 7 represent the adsorption isotherms of Pb(II), Cd(II), and Cu(II) at temperatures of 298, 308, and 318 K. It was found that the adsorption capacity of GO/

https://doi.org/10.1021/acsomega.1c06647
ACS Omega 2022, 7, 10944−10954

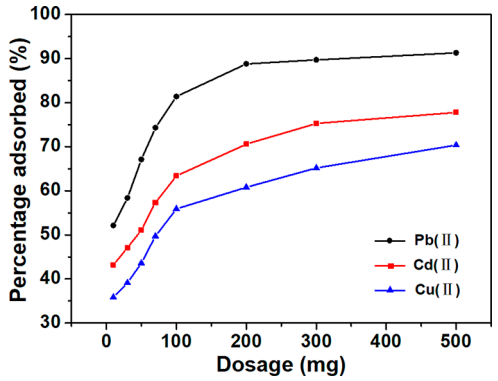

Figure 6. Effect of adsorbent (GO/HPAMAM/DAC) dosage on the adsorption of Pb(II), Cd(II), and Cu(II) (T = 298 K, t = 60 min, pH = 6.0, V = 50 mL, C_0^{metal} = 100 mg/L).

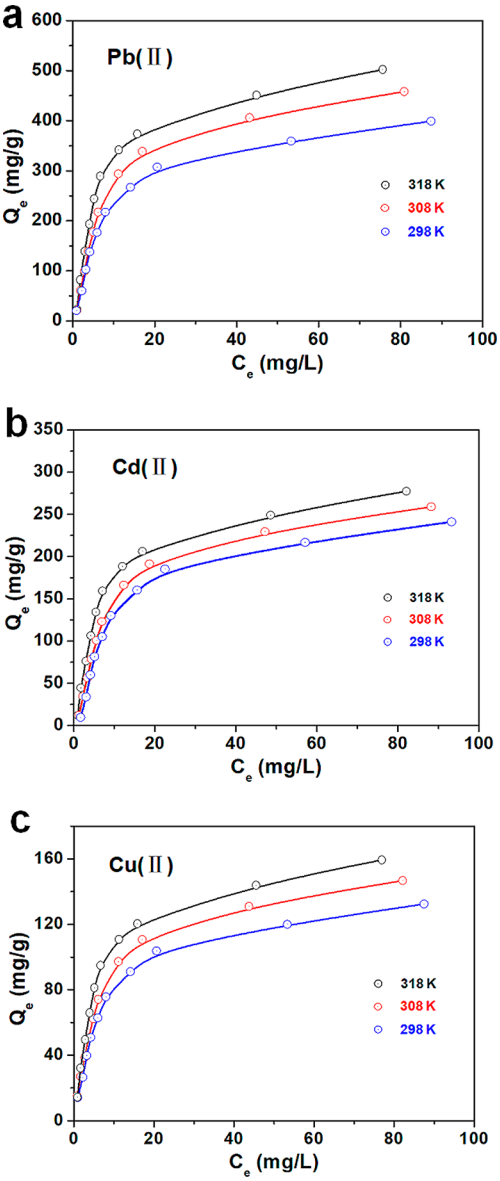

Figure 7. Adsorption isotherms of (a) Pb(II), (b) Cd(II), and (c) Cu(II) onto GO/HPAMAM/DAC at different temperatures (t = 24 h, m = 10 mg, V = 100 mL).

HPAMAM/DAC for heavy metal ions increased with the increase of temperature. During the adsorption process, it took a lot of energy to transfer Pb(II), Cd(II), and Cu(II) to the surface of GO/HPAMAM/DAC. Therefore, the high adsorption temperature improved the adsorption performance of GO/HPAMAM/DAC.

The adsorption kinetics of Pb(II), Cd(II), and Cu(II) onto GO/HPAMAM/DAC adsorbent at 298 K are shown in Figure 8a. There were two adsorption stages for these three

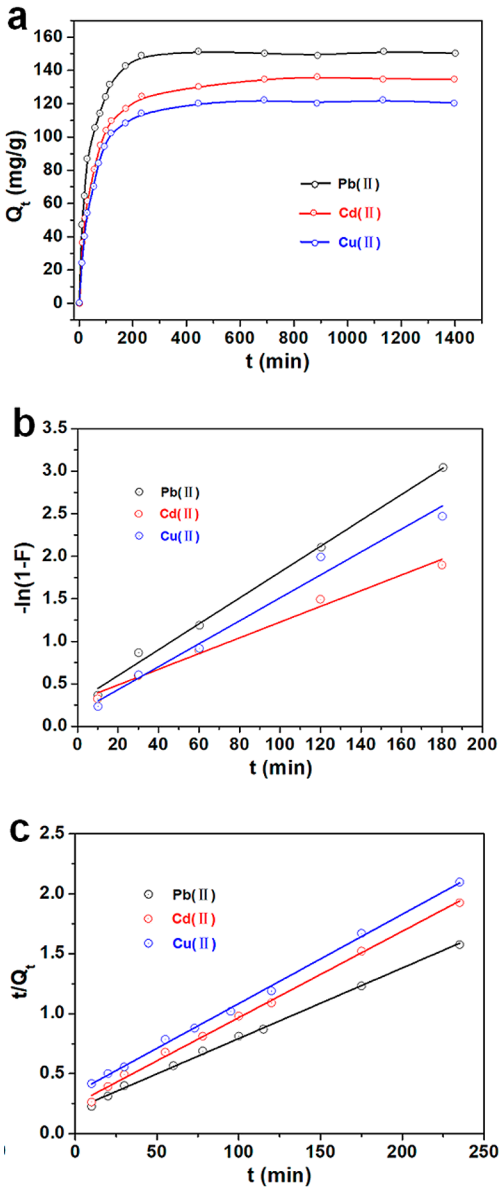

Figure 8. (a) Kinetic adsorption curve of GO/HPAMAM/DAC adsorbent for Pb(II), Cd(II), and Cu(II) (T = 298 K, t = 24 h, m = 10 mg, V = 100 mL, C_0^{metal} = 100 mg/L). (b) Pseudo-first-order kinetic model. (c) Pseudo-second-order kinetic model.

adsorbates. First, the adsorption capacity increased rapidly in the first 150 min. Then, the adsorption process tended to balance, and the adsorption capacity reached a stable level. A large number of active groups and micro/nano bumps in GO/HPAMAM/DAC increased its interaction with heavy metal ions. Pseudo-first-order and pseudo-second-order kinetics were fitted to measure the data to investigate the adsorption process.

https://doi.org/10.1021/acsomega.1c06647
ACS Omega 2022, 7, 10944−10954

Table 1. Adsorption Kinetic Parameters of Two Kinetic Models for Different Adsorbates

	pseudo-first-order			pseudo-second-order		
adsorbate	Q_e (mg/g)	k_1 (1/min)	R^2	k_2 (g/mg·min)	Q_e (mg/g)	R^2
Pb(II)	148.8	0.01522	0.9940	0.00017	169.8	0.9977
Cd(II)	131.6	0.00924	0.9857	0.00021	138.7	0.9970
Cu(II)	118.2	0.01349	0.9749	0.00016	134.2	0.9978

The Lagergren first-order rate equation based on the amount of solid adsorption is most commonly used. However, pseudo-first-order kinetics are only adapted to the primary stage of the adsorption process. The linear form of pseudo-first-order kinetics is discontinuous as soon as Q_e is attained. Therefore, only data points within 85% of Q_e were considered for modeling pseudo-first-order kinetics. The pseudo-first-order kinetics equation applied to the liquid phase is as follows:

$$-\ln(1 - F) = k_1 t + CF = \frac{Q_t}{Q_e} \quad (1)$$

where Q_t (mg/g) is the amount of heavy metal ions adsorbed at the contact time t (min), Q_e (mg/g) is the amount of heavy metal ions adsorbed at equilibrium, and k_1 (min^{-1}) is the kinetic rate constant. The curves of $-\ln(1 - F)$ vs t are shown in Figure 8b, and the k_1 values are displayed in Table 1.

The pseudo-second-order kinetic model is based on the assumption that the adsorption rate is controlled by chemical adsorption, which involves electron sharing or electron transfer between the adsorbate and the adsorbent. The pseudo-second-order kinetics is expressed as follows:

$$\frac{t}{Q_t} = \frac{1}{Q_e} t + \frac{1}{k_2 Q_e^2} \quad (2)$$

where k_2 (g mg^{-1} min^{-1}) is the kinetic rate constant. The curves of t/Q_t vs t are shown in Figure 8c, and the k_2 values are displayed in Table 1.

As shown in Table 1, the R^2 values of the pseudo-second-order kinetic model for Pb(II), Cd(II), and Cu(II) adsorption are all larger than those of the pseudo-first-order kinetic model. It confirms that the pseudo-second-order kinetic model best described the Pb(II), Cd(II), and Cu(II) adsorption onto the GO/HPAMAM/DAC adsorbent. The pseudo-second-order kinetic model is based on the hypothesis that the bimolecular interaction of ion-exchange between adsorbent and adsorbate is the rate-limiting step of adsorption.[12] On the basis of this, the adsorption of Pb(II), Cd(II), and Cu(II) onto GO/HPAMAM/DAC is through ionic interactions with hydroxyl groups on the surface of the adsorbent. The number of active sites on the adsorbent determined the adsorption capacity. The higher Q_e value of GO/HPAMAM/DAC (Table 1) for Pb(II) means a higher adsorption capacity and affinity, which was attributed to the stronger chemical interaction between GO/HPAMAM/DAC and Pb(II).

Figure 9a presents the adsorption isotherms of Pb(II), Cd(II), and Cu(II) onto GO/HPAMAM/DAC adsorbent at 298 K. The adsorption capacities of GO/HPAMAM/DAC adsorbent for Pb(II), Cd(II), and Cu(II) increased with the increase of the initial concentration of heavy metal ions. The GO/HPAMAM/DAC adsorbent exhibited the strongest adsorption capacity for Pb(II). The Langmuir and Freundlich isotherm models were used to demonstrate the adsorption process of GO/HPAMAM/DAC adsorbent for Pb(II), Cd(II), and Cu(II).

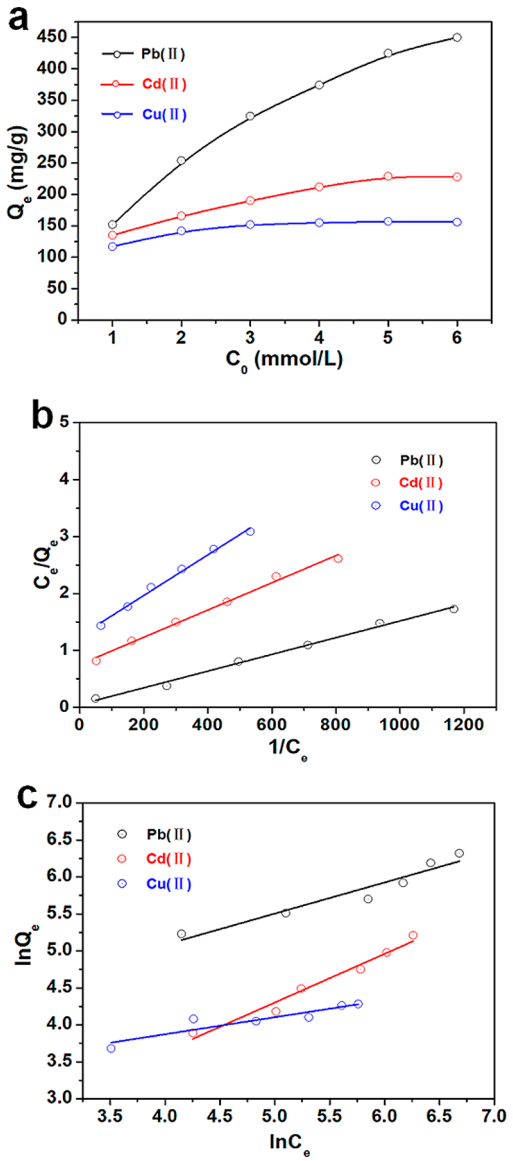

Figure 9. (a) Adsorption isotherms of GO/HPAMAM/DAC adsorbent for Pb(II), Cd(II), and Cu(II) (T = 298 K, t = 24 h, m = 10 mg, V = 100 mL). (b) Langmuir isotherm model. (c) Freundlich isotherm model.

The Langmuir model is based on the assumption that the adsorption of adsorbent on the adsorbent is homogeneous.[34] Adsorption occurs on the equivalent sites without interference from adjacent sites. The Langmuir isotherm is expressed as follows:

$$\frac{C_e}{Q_e} = \frac{C_e}{Q_m} + \frac{1}{bQ_m} \quad (3)$$

where Q_m (mg/g) represents the maximum adsorption capacity of unit weight adsorbent for heavy metal ions and b

https://doi.org/10.1021/acsomega.1c06647
ACS Omega 2022, 7, 10944−10954

Table 2. Adsorption Isotherm Parameters of Two Isotherm Models for Different Adsorbates

	Langmuir model			Freundlich model		
adsorbate	Q_m (mg/g)	b (L/mg)	R^2	k (mg/g)	n	R^2
Pb(II)	680.3	0.0284	0.9927	29.91	2.3737	0.9123
Cd(II)	418.4	0.0032	0.9909	2.74	1.5183	0.9648
Cu(II)	280.1	0.0028	0.9907	19.11	4.3397	0.8174

Table 3. Q_m for GO/HPAMAM/DAC Compared with Other Adsorbents Reported

	Q_m (mg/g)				
adsorbent	Pb(II)	Cd(II)	Cu(II)	temperature (K)	reference
graphene oxide/cellulose membranes	107.9	16.7	14.3	298	36
modified biochar			16.1	293	37
GO/CMC	76.7	46.1	82.9	293	23
lignosulfonate-graphene oxide-polyaniline	216.4			303	38
multimetal binding biosorbent	63.4	38.3	108.1	296	39
cross-linked grapheme oxide sheets via modified extracted cellulose	186.5		46.4	298	22
GO-HBP-NH_2−CMC	150.3		137.5	298	40
GO/HPAMAM/DAC	680.3	418.4	280.1	298	this work

(L/mg) is the Langmuir adsorption constant. The curves of C_e/Q_e vs $1/C_e$ are shown in Figure 9b, and the Q_m and b values are displayed in Table 2.

The Freundlich model is used to predict reversible and nonideal adsorption on heterogeneous adsorption sites, which does not form a monolayer on the surface of the adsorbent.[35] The Freundlich isotherm is expressed as follows:

$$\ln Q_e = \ln k + \frac{1}{n}\ln C_e \quad (4)$$

where k and n are Freundlich adsorption constants: k (mg/g) is a rough index for the adsorption capacity, $1/n$ represents the empirical parameter of adsorption intensity. The curves of ln Q_e vs ln C_e are shown in Figure 9c, and the k and n values are displayed in Table 2.

As shown in Table 2, the R^2 of the Langmuir isotherm model for Pb(II), Cd(II), and Cu(II) adsorption are larger than those of the Freundlich isotherm model. Therefore, it can be concluded that the Langmuir isotherm model best describes the Pb(II), Cd(II), and Cu(II) adsorption onto the GO/HPAMAM/DAC adsorbent. The Q_m values of Pb(II), Cd(II), and Cu(II) are 680.3, 418.4, and 280.1 mg/g at 298 K. The Q_m value for Pb(II) is higher than those of Cd(II) and Cu(II). This was attributed to the stronger chelation or complexation between GO/HPAMAM/DAC and Pb(II). Compared to most of the adsorbents listed in Table 3, the GO/HPAMAM/DAC adsorbent exhibits a higher Q_m for Pb(II), Cd(II), and Cu(II). All the above results confirm that GO/HPAMAM/DAC is a promising adsorbent for the adsorption of heavy metal ions.

In addition, cycling stability is an important factor that restricts the practical application of adsorbents. Adsorbents with a high adsorption capacity and good desorption capacity can reduce secondary pollution and also reduce the cost of preparing new adsorbents. Desorption experiments were performed by washing the adsorbent with NaOH and HCl. The adsorption capacities of the GO/HPAMAM/DAC adsorbent for Pb(II), Cd(II), and Cu(II) in five cycles are shown in Figure 10. Even after five cycles, more than 90% of Pb(II), Cd(II), and Cu(II) could be readsorbed. The good recycling performance of GO/HPAMAM/DAC adsorbent was attributed to the structural stability contributed by covalent grafting between GO, hyperbranched polymer, and cellulose.

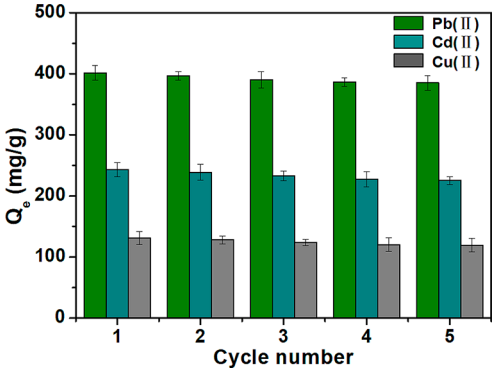

Figure 10. Adsorption capacities of GO/HPAMAM/DAC adsorbent for Pb(II), Cd(II), and Cu(II) in five cycles.

Adsorption Mechanism of GO/HPAMAM/DAC Adsorbent. The GO/HPAMAM/DAC adsorbent with a large number of active groups and micro/nano bumps showed strong adsorption capacity for heavy metal ions in wastewater. In fact, the adsorbent structure, ionic characteristic, and environmental conditions all have a great influence on the adsorption capacity of the adsorbent. To study the adsorption mechanism of GO/HPAMAM/DAC adsorbent, FT-IR and XPS were conducted to analyze the adsorption sites of the GO/HPAMAM/DAC adsorbent. The FT-IR spectra of GO/HPAMAM/DAC before and after heavy metal-ion adsorption are shown in Figure 11a. For GO/HPAMAM/DAC, the broad peak at 3000−3500 cm^{-1} was attributed to the superposition of O—H and N—H vibration, and the peaks at 1650 and 1558 cm^{-1} were ascribed to O═C—NH and C═N vibration. After the adsorption of Pb(II), Cd(II), and Cu(II), the peaks at 3000−3500 cm^{-1} tended to broaden. This confirmed that the hydroxyl and amino groups contributed to the adsorption of heavy metal ions. In addition, the peaks at 1650 and 1558 cm^{-1} were weakened, suggesting that the nitrogen- and oxygen-containing groups on GO/HAPAMAM/DAC adsorbent could chelate and/or compound heavy metal ions by acting as electron donors.

The XPS spectra of GO/HPAMAM/DAC before and after heavy metal-ion adsorption are shown in Figure 11b. Pb, Cd, and Cu appeared in XPS spectra after adsorption, confirming

https://doi.org/10.1021/acsomega.1c06647
ACS Omega 2022, 7, 10944−10954

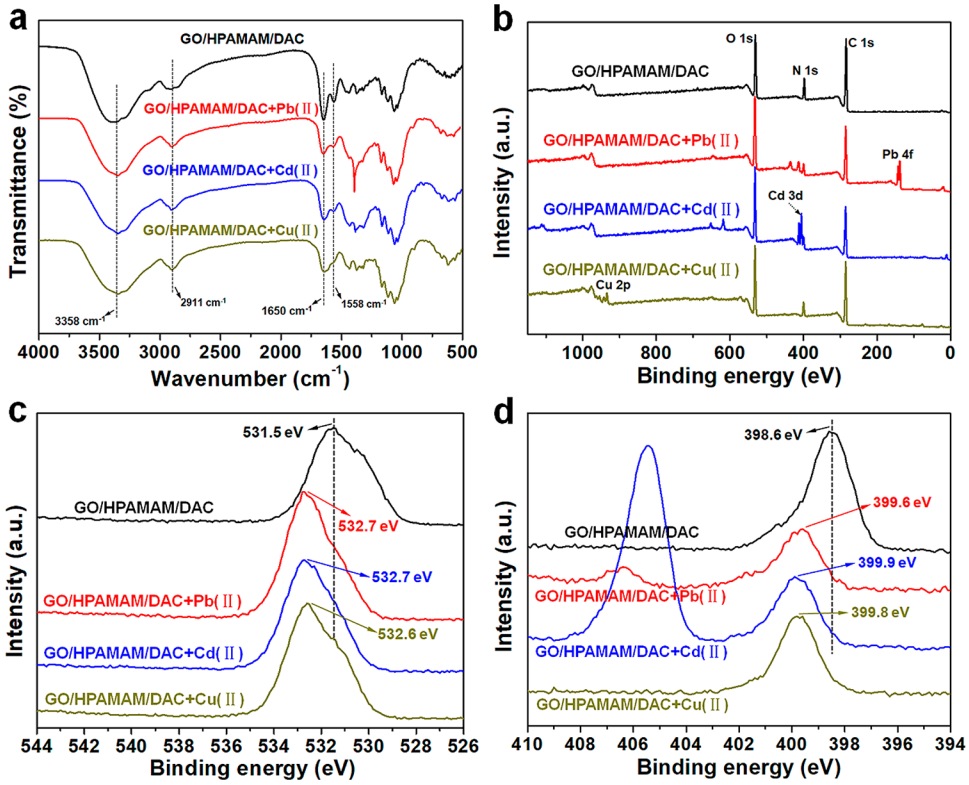

Figure 11. (a) FT-IR spectra of GO/HPAMAM/DAC before and after heavy metal ions adsorption. (b) Full XPS spectra of GO/HPAMAM/DAC before and after heavy metal ions adsorption, and high-resolution XPS spectra of (c) O 1s and (d) N 1s.

the pollutant adsorption on GO/HPAMAM/DAC. Parts c and d of Figure 11 show the O 1s and N 1s XPS spectra of GO/HPAMAM/DAC before and after Pb(II), Cd(II), and Cu(II) adsorption. For GO/HPAMAM/DAC, the peaks of O 1s and N 1s appeared at 531.5 and 398.6 eV. After adsorption, these two peaks moved toward high binding energy, indicating the interaction between oxygen-/nitrogen-containing groups and heavy metal ions in the adsorption process. This was consistent with the results of FT-IR. On the contrary, the terminal amino group of HPAMAM is naturally reducing, which can partially reduce the bound Pb(II), Cd(II), and Cu(II). Besides complexation, the removal of heavy metal ions was accompanied by the generation of metal ion derivatives (elemental and hydroxide) on GO/HPAMAM/DAC.

In addition, the morphology and adsorption sites of the adsorbent directly affect the adsorption capacities of Pb(II), Cd(II), and Cu(II) on GO/HPAMAM/DAC. The grafting of DAC with the help of HPAMAM built micro/nano bumps on GO, which greatly increased the contact area of adsorbent with the pollutants. On the contrary, the grafted cellulose provided more hydroxyl groups to GO, increasing the electrostatic interaction with heavy metal ions. Therefore, the grafting of DAC on GO improved the adsorbent morphology and increased the adsorption sites. This is also the reason the adsorption capacity of GO/HPAMAM/DAC is significantly improved.

CONCLUSIONS

In this study, hyperbranched polymers and cellulose were used to surface functionalized GO for the efficient adsorption of heavy metal ions. HPAMAM was covalently grafted onto GO via amide bonds, increasing the active groups on the GO surface and enhancing the affinity with heavy metal ions. DAC was covalently grafted onto GO/HPAMAM by forming a Schiff-based structure with HPAMAM. Interestingly, DAC formed micro/nano bumps on GO, which was beneficial to increase the hydroxyl number and contact area with heavy metal ions. The maximum adsorption capacities of GO/HPAMAM/DAC for Pb(II), Cd(II), and Cu(II) were 680.3, 418.4, and 280.1 mg/g at 298 K, which were better than those of most adsorbents reported. In addition, GO/HPAMAM/DAC exhibited good cyclic adsorption stability for heavy metal ions. A pseudo-second-order kinetic model could well-describe the Pb(II), Cd(II), and Cu(II) adsorption onto GO/HPAMAM/DAC, and the equilibrium data fitted well with the Langmuir isotherm model. The adsorption mechanism was mainly reflected in the chelation or complexation of heavy metal ions by nitrogen- and oxygen-containing groups on GO/HPAMAM/DAC. This study may provide a novel strategy for improving the adsorption performance of GO with hyperbranched polymers and cellulose.

EXPERIMENTAL SECTION

Materials. The GO was obtained from Deke Daojin Science and Technology Co., Ltd. (Beijing, China). The HPAMAM was purchased from Hyperbranched Polymers Science & Technology Co., Ltd. (Wuhan, China). The molecular weight of HPAMAM was about 1900−2200 g/mo,l and the amino amount was about 12−16 mol/mol. The MCC was provided by Yuanye Biotechnology Co., Ltd. (Shanghai, China). The crystallinity of MCC was 62.9%, and the degree of polymerization was 200−250. The HCl, NaOH, $NaIO_4$, 1-(3-dimethylaminopropyl)-3-ethylcarbodiimide (EDC), *N*-hydroxysuccinimide (NHS), $Pb(NO_3)_2$, $Cd(NO_3)_2$,

https://doi.org/10.1021/acsomega.1c06647
ACS Omega 2022, 7, 10944−10954

and $Cu(NO_3)_2$ were purchased from Maclin Biochemical Technology Co., Ltd. (Shanghai, China).

Synthesis of GO/HPAMAM/DAC Adsorbent. Typically, GO (0.1 g) was dispersed in deionized water (50 mL) with the help of ultrasonic vibration. The HPAMAM (1 g) was then added to the GO dispersion and reacted at 70 °C for 1 h in the presence of EDC/NHS catalyst to obtain GO/HPAMAM complex.[16,17] On the contrary, 20 mL of deionized water was used to disperse 1 g of MCC. Then, 1 g of $NaIO_4$ was added to MCC dispersion, and the pH was adjusted to 3.0 with 0.1 mol/L HCl. After which, the mixture reacted at 30 °C for 8 h in the dark to obtain dialdehyde cellulose (DAC). After filtration and washing, DAC was added to the GO/HPAMAM complex and reacted at 70 °C for 6 h. Subsequently, the mixture was washed, filtered, and dried to obtain the GO/HPAMAM/DAC adsorbent.

Characterization. A Vertex 80 V spectrophotometer (Bruker) in the range 4000−500 cm^{-1} was used to acquire the FT-IR spectra with a can speed of 4 cm^{-1}. The XRD patterns were carried out with an Ultima IV X-ray diffractometer (Rigaku) in the range 5°90° (2θ) with Cu Kα radiation at 40 mA and 40 kV. The XPS spectra were conducted in an Axis Ultra^{DLD} X-ray photoelectron spectrometer (Kratos) using Mg Kα ($h\gamma$ = 1253.6 eV) as the radiation source. Thermogravimetric analysis (TGA) was carried out on a Q-500 thermogravimetric analyzer. Approximately 5 mg of each sample was heated under nitrogen gas at a rate of 10 °C/min. The gas adsorption isotherms were obtained with a Quantachrome Autosorb-iQ (Micro 2460). About 0.2 g of sample was degassed at 120 °C for 7 h. The SEM images were taken using a Supra 55 field-emission scanning electron microscope (Zeiss). The ζ potentials of GO/HPAMAM/DAC suspension were detected in a Nano-ZS90 Zetasizer (Malvern).

Adsorption Experiments. Typically, heavy metal ion solutions (100 mL) of Pb(II), Cd(II), or Cu(II) were mixed with 10 mg of GO/HPAMAM/DAC adsorbent and stirred for 24 h at 298 K. The adsorption experiment was carried out multiple times with different initial concentrations, temperatures, dosages, and pH values. After that, the GO/HPAMAM/DAC adsorbent was separated from the mixture using a 0.22 μm membrane. An AA-6300C atomic adsorption spectrometer (Shimadzu) was used to quantitatively detect the content of heavy metal ions in the filtrate. For cyclic adsorption experiments, 0.1 mol/L NaOH and 0.1 mol/L HCl were utilized to desorb Pb(II), Cd(II), and Cu(II) from GO/HPAMAM/DAC. The adsorbents were washed four times with deionized water after desorption to neutralize the pH of solution. Finally, the adsorbents were dried at 60 °C in a vacuum oven.

AUTHOR INFORMATION

Corresponding Author

Xiujie Huang − *Key Laboratory of Bio-based Material Science & Technology (Northeast Forestry University), Ministry of Education, Harbin 150040, China;* orcid.org/0000-0002-1694-0609; Phone: +86−0451—82190394; Email: shanmu1128@163.com

Authors

Zhihang Liu − *Key Laboratory of Bio-based Material Science & Technology (Northeast Forestry University), Ministry of Education, Harbin 150040, China*

Qian Wang − *Key Laboratory of Bio-based Material Science & Technology (Northeast Forestry University), Ministry of Education, Harbin 150040, China*

Xueren Qian − *Key Laboratory of Bio-based Material Science & Technology (Northeast Forestry University), Ministry of Education, Harbin 150040, China*

Complete contact information is available at: https://pubs.acs.org/10.1021/acsomega.1c06647

Notes

The authors declare no competing financial interest.

ACKNOWLEDGMENTS

This work was financially supported by the Young Elite Scientists Sponsorship Program by CAST (2018QNRC001), the Fundamental Research Funds for the Central Universities (2572019BB01), and the Research Training Program of Undergraduate Students in Northeast Forestry University (202010225054).

REFERENCES

(1) Uogintė, I.; Lujanienė, G.; Mažeika, K. Study of Cu (II), Co (II), Ni (II) and Pb (II) removal from aqueous solutions using magnetic Prussian blue nano-sorbent. *J. Hazard. Mater.* **2019**, *369*, 226−235.

(2) Madadrang, C. J.; Kim, H. Y.; Gao, G.; Wang, N.; Zhu, J.; Feng, H.; Gorring, M.; Kasner, M. L.; Hou, S. Adsorption behavior of EDTA-graphene oxide for Pb (II) removal. *ACS Appl. Mater. Interfaces* **2012**, *4* (3), 1186−1193.

(3) Barakat, M. A. New trends in removing heavy metals from industrial wastewater. *Arab. J. Chem.* **2011**, *4* (4), 361−377.

(4) Mehdaoui, R.; Chaabane, L.; Beyou, E.; Baouab, M. H. V. Sono-heterogeneous Fenton system for degradation of AB74 dye over a new tetraaza macrocyclic Schiff base cellulose ligand-loaded Fe_3O_4 nanoparticles. *J. Iran. Chem. Soc.* **2019**, *16* (3), 645−659.

(5) Xiang, B.; Ling, D.; Lou, H.; Gu, H. 3D hierarchical flower-like nickel ferrite/manganese dioxide toward lead (II) removal from aqueous water. *J. Hazard. Mater.* **2017**, *325*, 178−188.

(6) Duru, İ.; Ege, D.; Kamali, A. R. Graphene oxides for removal of heavy and precious metals from wastewater. *J. Mater. Sci.* **2016**, *51* (13), 6097−6116.

(7) Zhao, G.; Huang, X.; Tang, Z.; Huang, Q.; Niu, F.; Wang, X. Polymer-based nanocomposites for heavy metal ions removal from aqueous solution: a review. *Polym. Chem.* **2018**, *9* (26), 3562−3582.

(8) Srinivasan, B. M.; Hao, Y.; Hariharaputran, R.; Rywkin, S.; Hone, J. C.; Colombo, L.; Ruoff, R. S.; Zhang, Y. W. Oxygen-promoted chemical vapor deposition of graphene on copper: a combined modeling and experimental study. *ACS Nano* **2018**, *12* (9), 9372−9380.

(9) Pazat, A.; Beyou, E.; Barrès, C.; Bruno, F.; Janin, C. In situ emulsion cationic polymerization of isoprene onto the surface of graphite oxide sheets. *Appl. Surf. Sci.* **2017**, *396*, 902−911.

(10) Cui, L.; Wang, Y.; Gao, L.; Hu, L.; Yan, L.; Wei, Q.; Du, B. EDTA functionalized magnetic graphene oxide for removal of Pb (II), Hg (II) and Cu (II) in water treatment: adsorption mechanism and separation property. *Chem. Eng. J.* **2015**, *281*, 1−10.

(11) Akpotu, S. O.; Moodley, B. Encapsulation of silica nanotubes from elephant grass with graphene oxide/reduced graphene oxide and its application in remediation of sulfamethoxazole from aqueous media. *ACS Sustain. Chem. Eng.* **2018**, *6* (4), 4539−4548.

(12) Akpotu, S. O.; Moodley, B. Application of as-synthesised MCM-41 and MCM-41 wrapped with reduced graphene oxide/graphene oxide in the remediation of acetaminophen and aspirin from aqueous system. *J. Environ. Manage.* **2018**, *209*, 205−215.

(13) Manna, A.; Imae, T.; Aoi, K.; Okada, M.; Yogo, T. Synthesis of dendrimer-passivated noble metal nanoparticles in a polar medium:

comparison of size between silver and gold particles. *Chem. Mater.* **2001**, *13* (5), 1674−1681.
(14) Rehim, M. H. A.; Ismail, N.; Badawy, A. E. R. A.; Turky, G. Hydrogen storing and electrical properties of hyperbranched polymers-based nanoporous materials. *Mater. Sci. Eng., B* **2011**, *176* (15), 1184−1189.
(15) Huang, Z. W.; Li, Z. J.; Wu, Q. Y.; Zheng, L. R.; Zhou, L. M.; Chai, Z. F.; Wang, X. L.; Shi, W. Q. Simultaneous elimination of cationic uranium (VI) and anionic rhenium (VII) by graphene oxide-poly (ethyleneimine) macrostructures: a batch, XPS, EXAFS, and DFT combined study. *Environ. Sci. Nano* **2018**, *5* (9), 2077−2087.
(16) Akpotu, S. O.; Lawal, I. A.; Moodley, B.; Ofomaja, A. E. Covalently linked graphene oxide/reduced graphene oxide-methoxylether polyethylene glycol functionalised silica for scavenging of estrogen: Adsorption performance and mechanism. *Chemosphere* **2020**, *246*, 125729.
(17) Xikhongelo, R. V.; Mtunzi, F. M.; Diagboya, P. N.; Olu-Owolabi, B. I.; Düring, R.-A. Polyamidoamine-Functionalized Graphene Oxide-SBA-15 Mesoporous Composite: Adsorbent for Aqueous Arsenite, Cadmium, Ciprofloxacin, Ivermectin, and Tetracycline. *Ind. Eng. Chem. Res.* **2021**, *60* (10), 3957−3968.
(18) Yu, D.; Wang, Y.; Wu, M.; Zhang, L.; Wang, L.; Ni, H. Surface functionalization of cellulose with hyperbranched polyamide for efficient adsorption of organic dyes and heavy metals. *J. Clean. Prod.* **2019**, *232*, 774−783.
(19) Xue, F.; He, H.; Zhou, H.; Quan, Z.; Chen, Z.; Wu, Q.; Zhu, H.; Wang, S. Structural design of a cellulose-based hyperbranched adsorbent for the rapid and complete removal of Cr (VI) from water. *Chem. Eng. J.* **2021**, *417*, 128037.
(20) Zhao, B.; Jiang, H.; Lin, Z.; Xu, S.; Xie, J.; Zhang, A. Preparation of acrylamide/acrylic acid cellulose hydrogels for the adsorption of heavy metal ions. *Carbohydr. Polym.* **2019**, *224*, 115022.
(21) Qiao, L.; Li, S.; Li, Y.; Liu, Y.; Du, K. Fabrication of superporous cellulose beads via enhanced inner cross-linked linkages for high efficient adsorption of heavy metal ions. *J. Clean. Prod.* **2020**, *253*, 120017.
(22) Yakout, A. A.; El-Sokkary, R. H.; Shreadah, M. A.; Hamid, O. G. A. Cross-linked graphene oxide sheets via modified extracted cellulose with high metal adsorption. *Carbohyd. Polym.* **2017**, *172*, 20−27.
(23) Zhang, Y.; Liu, Y.; Wang, X.; Sun, Z.; Ma, J.; Wu, T.; Xing, F.; Gao, J. Porous graphene oxide/carboxymethyl cellulose monoliths, with high metal ion adsorption. *Carbohyd. Polym.* **2014**, *101*, 392−400.
(24) Zaman, A.; Orasugh, J. T.; Banerjee, P.; Dutta, S.; Ali, M. S.; Das, D.; Bhattacharya, A.; Chattopadhyay, D. Facile one-pot in-situ synthesis of novel graphene oxide-cellulose nanocomposite for enhanced azo dye adsorption at optimized conditions. *Carbohyd. Polym.* **2020**, *246*, 116661.
(25) Qi, Y.; Yang, M.; Xu, W.; He, S.; Men, Y. Natural polysaccharides-modified graphene oxide for adsorption of organic dyes from aqueous solutions. *J. Colloid Interface Sci.* **2017**, *486*, 84−96.
(26) Zhu, W.; Liu, L.; Liao, Q.; Chen, X.; Qian, Z.; Shen, J.; Liang, J.; Yao, J. Functionalization of cellulose with hyperbranched polyethylenimine for selective dye adsorption and separation. *Cellulose* **2016**, *23* (6), 3785−3797.
(27) Zeng, Y. L.; Huang, Y. F.; Jiang, J. H.; Zhang, X. B.; Tang, C. R.; Shen, G. L.; Yu, R. Q. Functionalization of multi-walled carbon nanotubes with poly (amidoamine) dendrimer for mediator-free glucose biosensor. *Electrochem. Commun.* **2007**, *9* (1), 185−190.
(28) Lv, J.; Zhang, G.; Zhang, H.; Yang, F. Graphene oxide-cellulose nanocrystal (GO-CNC) composite functionalized PVDF membrane with improved antifouling performance in MBR: Behavior and mechanism. *Chem. Eng. J.* **2018**, *352*, 765−773.
(29) Liu, Z.; Li, D.; Dai, H.; Huang, H. Enhanced properties of tea residue cellulose hydrogels by addition of graphene oxide. *J. Mol. Liq.* **2017**, *244*, 110−116.
(30) He, H.; Zhuang, L.; Chen, S.; Liu, H.; Li, Q. Structure design of a hyperbranched polyamine adsorbent for CO_2 adsorption. *Green Chem.* **2016**, *18* (21), 5859−5869.
(31) Liu, X.; Zhang, H.; Ma, Y.; Wu, X.; Meng, L.; Guo, Y.; Yu, G.; Liu, Y. Graphene-coated silica as a highly efficient sorbent for residual organophosphorus pesticides in water. *J. Mater. Chem. A* **2013**, *1* (5), 1875−1884.
(32) Wang, S.; Liu, Q.; Luo, Z.; Wen, L.; Cen, K. Mechanism study on cellulose pyrolysis using thermogravimetric analysis coupled with infrared spectroscopy. *Front. Energy* **2007**, *1* (4), 413−419.
(33) Hao, Y.; Cui, Y.; Peng, J.; Zhao, N.; Li, S.; Zhai, M. Preparation of graphene oxide/cellulose composites in ionic liquid for Ce (III) removal. *Carbohydr. Polym.* **2019**, *208*, 269−275.
(34) Akpotu, S. O.; Moodley, B. Synthesis and characterization of citric acid grafted MCM-41 and its adsorption of cationic dyes. *J. Environ. Chem. Eng.* **2016**, *4* (4), 4503−4513.
(35) Olu-Owolabi, B. I.; Popoola, D. B.; Unuabonah, E. I. Removal of Cu^{2+} and Cd^{2+} from aqueous solution by bentonite clay modified with binary mixture of goethite and humic acid. *Water Air Soil Pollut.* **2010**, *211* (1), 459−474.
(36) Sitko, R.; Musielak, M.; Zawisza, B.; Talik, E.; Gagor, A. Graphene oxide/cellulose membranes in adsorption of divalent metal ions. *RSC Adv.* **2016**, *6* (99), 96595−96605.
(37) Yang, G. X.; Jiang, H. Amino modification of biochar for enhanced adsorption of copper ions from synthetic wastewater. *Water Res.* **2014**, *48*, 396−405.
(38) Yang, J.; Wu, J. X.; Lu, Q. F.; Lin, T. T. Facile preparation of lignosulfonate-graphene oxide-polyaniline ternary nanocomposite as an effective adsorbent for Pb (II) ions. *ACS Sustain. Chem. Eng.* **2014**, *2* (5), 1203−1211.
(39) Abdolali, A.; Ngo, H. H.; Guo, W.; Zhou, J. L.; Zhang, J.; Liang, S.; Chang, S. W.; Nguyen, D. D.; Liu, Y. Application of a breakthrough biosorbent for removing heavy metals from synthetic and real wastewaters in a lab-scale continuous fixed-bed column. *Bioresour. Technol.* **2017**, *229*, 78−87.
(40) Kong, Q.; Preis, S.; Li, L.; Luo, P.; Hu, Y.; Wei, C. Graphene oxide-terminated hyperbranched amino polymer-carboxymethyl cellulose ternary nanocomposite for efficient removal of heavy metals from aqueous solutions. *Int. J. Biol. Macromol.* **2020**, *149*, 581−592.

https://doi.org/10.1021/acsomega.1c06647
ACS Omega 2022, 7, 10944−10954